Multispectral Single-Sensor RGB-NIR Imaging: New Challenges and Opportunities

Xavier Soria[1,3]
[1]*Computer Vision Center*
Edifici O Campus UAB
08193 Bellaterra
Barcelona, Spain
xsoria@cvc.uab.es

Angel D. Sappa[1,2]
[2]*Escuela Superior Politécnica del Litoral, ESPOL, Facultad de Ingeniería en Electricidad y Computación, CIDIS,* Campus Gustavo Galindo
Guayaquil, Ecuador
sappa@ieee.org

Arash Akbarinia[1,3]
[3]*Department of Computer Science, Autonomous University of Barcelona*
08193 Bellaterra
Barcelona, Spain
arash.akbarinia@cvc.uab.es

***Abstract*—Multispectral images captured with a single sensor camera have become an attractive alternative for numerous computer vision applications. However, in order to fully exploit their potentials, the color restoration problem (RGB representation) should be addressed. This problem is more evident in outdoor scenarios containing vegetation, living beings, or specular materials. The problem of color distortion emerges from the sensitivity of sensors due to the overlap of visible and near infrared spectral bands. This paper empirically evaluates the variability of the near infrared (NIR) information with respect to the changes of light throughout the day. A tiny neural network is proposed to restore the RGB color representation from the given RGBN (Red, Green, Blue, NIR) images. In order to evaluate the proposed algorithm, different experiments on a RGBN outdoor dataset are conducted, which include various challenging cases. The obtained result shows the challenge and the importance of addressing color restoration in single sensor multispectral images.**

***Index Terms*—Color restoration; Neural networks; Single-sensor cameras; Multispectral images; RGB-NIR dataset.**

I. Introduction

The computer vision field is rapidly expanding in different directions. Among all, the recent technological advancements in the hardware capabilities of cameras have triggered many new opportunities in a wide range of applications. At present, there are modern sensors that are capable of simultaneously capturing the visual information in different spectral bands far beyond the humans' visible spectrum. For instance, off-the-shelf multispectral (MS) single sensors [1], which cover both the visible and near infrared (NIR) spectral band (wavelength range of 400 to 1200 nm), can be bought for less than one hundred dollars. Moreover, thanks to modern computational units, a large bulk of information can be processed in just a few seconds. Hence, classical image processing algorithms, such as dehazing, enhancement, fusion, segmentation etc. (e.g., [2], [3], [4]), can take advantage of MS technology. Additionally, RGBN images can be also used in applications related with monitoring vegetation penology [5], visualization of subsurface blood vessels [6] or clean the haze in visible channel [7], to name a few.

Currently, most of the examples mentioned above are based on the usage of two cameras, one for the visible and another for the NIR spectrum. Consequently, any further visual information processing becomes conditional to the quality of the camera calibration and image registration. These overheads can be avoided by using single sensor cameras that record the RGB and NIR signal of the scene at one shot. The drawback of these cameras is that an unknown percentage of NIR information is also captured by the RGB sensor. This phenomenon is referred in the literature to as cross-talk between the RGB and NIR [8]. This issue can cause scattering or over absorption and reflectance from the captured surfaces [9]. Hence, interpolation or demosaicing are not enough to correct the impact of the NIR signal on the RGB colors, particularly in scenes containing vegetation or materials producing different reflection in the NIR spectra.

Fig. 1(a) illustrates an example of the issues mentioned above: colours appears to be de-saturated in an outdoor image that is illuminated with an intense sunlight near the infrared radiation. More details of this problem can be observed in the vegetation area. In the metabolism of healthy plants, energy from the blue and red lights is absorbed by the green chlorophyll pigments to fuel the photosynthesis process. Consequently, plants with more chlorophyll pigments reflect more NIR energy. In Fig. 1(c) it can be noticed that the R, G, and B bands expand through 700 nm to 1100 nm wavelength. This overlapping problem is present in single sensors cameras, therefore in order to obtain a typical RGB image, it is necessary to subtract the NIR information from the chromatic channels. This action will be referred throughout this paper as RGB color restoration, a term commonly used in the literature.

This paper presents an empirical evaluation of the variability of the NIR information according to the daylight time; this to certain extents demonstrate the need to continuously update the function of color restoration. In the current work a solution based on a tiny neural network is proposed to restore RGB

This work has been partially supported by the Spanish Government under Project TIN2014-56919-C3-2-R; by the "CERCA Programme / Generalitat de Catalunya"; and by the ESPOL project PRAIM. Arash Akbarinia has been supported by Universitat Autònoma de Barcelona. Xavier Soria would like to thank to Ecuador government institutions: SENESCYT under a scholarship contract 2015-AR3R7694 and Ministry of Education.

(a)

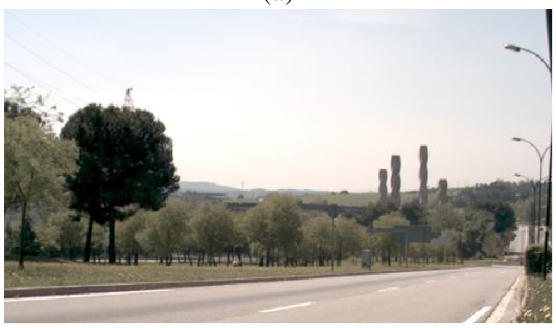

(b)

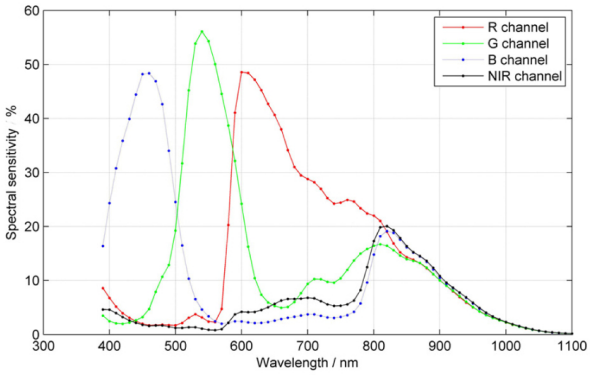

(c)

Fig. 1. (a) RGB image with near infrared infection (note how green color vegetation appears distorted by NIR information). (b) A typical RGB image of the same scene. (c) Spectral sensibility graph [1].

color images. A special dataset has been created and utilized for evaluation (i.e., any given scene was captured a number of times throughout the day in order to faithfully represent the changes of NIR information). The rest of the paper is organized as follows. In Section II, at first, previous works on multispectral imaging are summarized, after that the details of the collected dataset is described; this is followed by Section III which presents the proposed approach to restore RGB colors. The results of conducted experiments are reported in Section IV; and finally, Section V concludes this article.

II. Related Work

This section presents state-of-the-art on works related to RGB color restoration from RGBN single sensor multispectral images, as well as on single sensor MS image datasets. These datasets are intended to cover topics related to the sensor, the surface of the objects in the scene or the illumination influence [10], which are highly related to the color restoration problem.

A. RGB Image Color Restoration

In 2013, Yan *et al.* [11] published a multispectral image restoration exploring a via scale map approach, which was extended in [12]. Such scale map s captures the nature of structure discrepancy between images and has a clear statistical and numerical meaning. A noisy RGB image (I_0) is taken as an input to the system; next, by using a guidance image (G), which is captured from the same camera position, an output image without noise is created. The s was introduced too as auxiliary with the same size as G. Such a map was the key contribution of that approach to adapt the structure of G to that of I^* (the ground truth noise-free image). In other works s is a ratio map between G and the I^*.

In a recent work [1], the white balance, chromatic adaptation and color correction matrix (CCM), were used to form a RGB color correction whenever such channels have cross-talking with NIR. The CCM was obtained by using a x-rite color checker chart as color calibration target. In [13], as well as in [8] and [14], authors proposed the following pipeline for color correction: modified color filter array, interpolation, demosaicing and color correction matrix. Such techniques have special configuration or adaptation because of the additional NIR sensor.

The RGB color restoration problem has also been addressed in [15] as a more detailed extension of [16]. Authors developed an algorithm focusing on spectral estimation and decomposition, in other words, by using signal processing approaches they estimated the NIR band response in each of the RGBN channels. On the other hand, in the spectral decomposition stage, the unknown value in N_{VIS} and N_{NIR} were also estimated. Two single sensor multispectral cameras were used to evaluate this approach; one with Infrared Cut Off Filter (IRCF), the other without IRCF, and a standard color in the Macbeth SG color checker chart was used for the training set to compute the correlation coefficients in spectral estimation stage.

B. MS Image Datasets

In recent years, the number of datasets containing RGBN images has increased (e.g., [17], [18]). The major differences among current datasets is their field of application as mentioned in Section I. Nevertheless, usually their images are acquired at least by two cameras and not by modern single sensors. To the best of our knowledge, there are only a few outdoor single sensor MS datasets publicly available and there is a lack of a benchmark dataset to evaluate color correction algorithms in a common fashion. Gathering a large set of images not only is necessary to quantitatively evaluate different algorithms, but also it allows for machine learning approaches to have sufficient data for their training procedures.

Most of the previous works in the literature, discussed above, were evaluated primarily with MS images captured

in fully controlled indoor scenes, without the presence of any vegetation or specular materials. In [13], [8] and [12] authors included only a few outdoor images and there are no clear indications of how the NIR overlapping problem was tackled in order to remove its contamination from the RGB channels. In a recent work [19], an algorithm was proposed to recover RGB images from outdoor images of RGBN format that are illuminated with sufficient sun infrared radiation. The color restoration approach proposed in [19] is grounded on a Neural Network (NN)—a tiny feed-forward network (multilayer perceptron).

In order to have a benchmark for color restoration approaches we present a set of MS outdoor images captured under sufficient sunlight covering a wide range of challenging conditions[1]. The dataset is organized in three categories: 1) outdoor MS images with vegetation (OMSIV), which contains images from different scenarios containing vegetation; 2) outdoor MS images without vegetation (OMSINV), which contains images from different scenarios without vegetation; and 3) whole day single-scene outdoor MS images (SSOMSI), which contains images of the same scenario obtained throughout the whole day; the last category is intended to evaluate the image formation according to the light and sensor sensitivity.

The entire dataset (SSMID: single sensor multispectral image dataset) was captured with a 4 megapixels MS camera. Each MS image is supplemented with its corresponding "visible" image captured with the same camera but with an Infrared Cut Off Filter (IRCF), which blocks the IR light radiation. The original images are in a RAW format and they have to be converted into RGBN images. The size of each RAW image is 1280x720 pixels, and after its channels are separated, the size becomes 640x360x4 for the RGBN and 640x360x3 for the RGB (visible channels without the NIR information). In order to guarantee overlap between RGBN images and their corresponding RGB (obtained with IRCF) the images have been cropped to a square of 256x256x4. These cropped regions have been registered using [20], in order to have ground truth values (corrected color for every pixel).

The SSMID dataset contains 744 pairs of MS images (including both the RGBN and their corresponding RGB for ground truth). It is composed of: 533 pairs in OMSIV; 61 pairs in OMSINV; and 150 pairs in SSOMSI. All images were acquired in scenes with sun infrared radiation. The SSMID images were captured in university campus and city areas between January and April 2017. As mentioned above, the dataset is fully available for downloading to develop and evaluate RGB color restoration approaches, as well as other MS image processing algorithms (e.g., image enhancement, noise filtering, etc.).

III. RGB Color Image Restoration based on NN

Formation of a chromatic image with three colour channels depends on at least three factors [10], [21]: light source $e(\lambda)$, surface reflectance $r(\lambda)$ and camera sensitivity $c(\lambda)$, which in turn $c(\lambda) = \{R(\lambda), G(\lambda), B(\lambda)\}$. Placing all the pieces together, an image I can be defined as:

$$I = \int_w e(\lambda) r(\lambda) c^{(k)}(\lambda) d\lambda \ , \tag{1}$$

where k is the number of bands captured by the MS camera sensor. Therefore, a MS image captured with a single sensor (RGBN) is obtained as follow:

$$I = [R_{VIS+NIR}, G_{VIS+NIR}, B_{VIS+NIR}, NIR_{NIR}]^T, \tag{2}$$

where VIS is the visible spectral band (400 - 700 nm). The band overlap problem can be observed in the plot presented Fig. 1(c), note that according to the provider of MS camera used in the current work, NIR is not affected by (R,G,B) channels. The objective of the RGB color restoration is to get an image in the visible spectral band ($\hat{I} = [R_{VIS}, G_{VIS}, B_{VIS}]$ from Eq. 2) as perceived by the human visual perception system (similar to the picture of 1(b)). According to Eq. 1 there are three factors that affect the amount of NIR information in the visible channels. All of them (light source, surface reflectance and camera sensitivity) play an important and unknown role for the MS image formation. In order to empirically evaluate the impact of light source and camera sensitivity, in the SSOMSI dataset we have captured an outdoor scene during the whole day.

Fig. 2 showcases challenges of color restoration originated from the variation of illumination throughout the day. It can be observed from Fig. 2(a) that the lighting variation is significant at different hours of a day. These variations result in different amount of influence from the NIR information to the RGB channels, which directly impact the angular error (AE) values when RGBN images are compared with their corresponding RGB ones (Fig. 2(b)).

Fig. 3 presents two sample RGBN images (*the top row*) along with their corresponding RGB images (*the middle row*) that are used as ground truth. These pictures have been acquired from the same scenario but at different times of the day. This time difference can be observed in the amount of NIR information present in the scene (*the bottom row*), which can disturb the color formation (compare Fig. 3 (a) with (b)). In order to obtain the RGB image without NIR affection ($\hat{I}_{VIS}$) the NIR component need to be removed from each channel:

$$\begin{bmatrix} \hat{R}_{VIS} \\ \hat{G}_{VIS} \\ \hat{B}_{VIS} \end{bmatrix} = \begin{bmatrix} R_{VIS+NIR} - \alpha N_{NIR} \\ G_{VIS+NIR} - \beta N_{NIR} \\ B_{VIS+NIR} - \gamma N_{NIR} \end{bmatrix} \tag{3}$$

where α, β and γ are the respective unknown NIR percentages in each channel; their values are variables depending on the objects' surface reflectance and light source. These values can be in the range of $[-1, 1]$. In the current work, in order to restore an image with unknown percentages of NIR information, we propose to use a tiny neural network (NN). The architecture of this NN is used as a regressor and trained

[1]The collected dataset is available online under this link: https://xavysp.github.io/publication/paperIPTA2017.

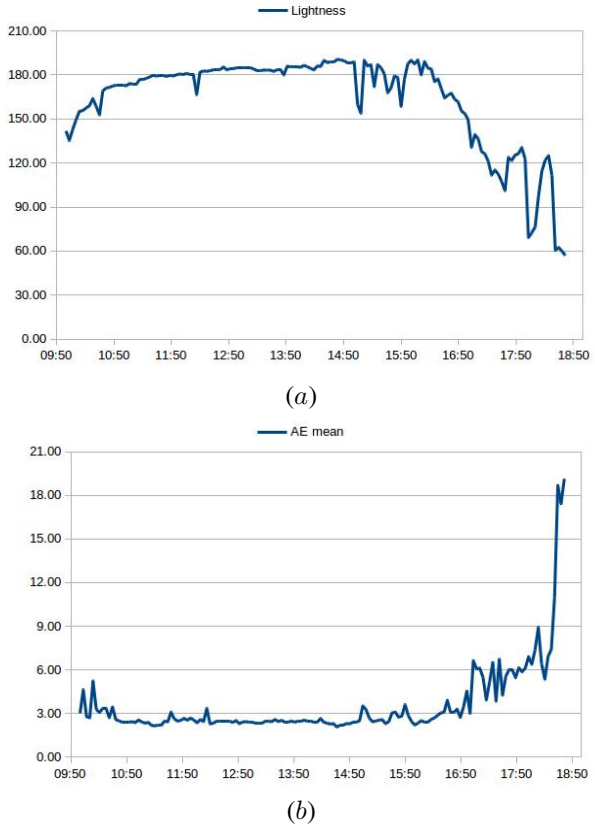

Fig. 2. (a) Lightness of each of the images captured in a given scene from 10 AM till 6:50 PM. (b) Mean of Angular Error (AE) computed from each RGBN image and the corresponding RGB (ground truth obtained with the IRCF).

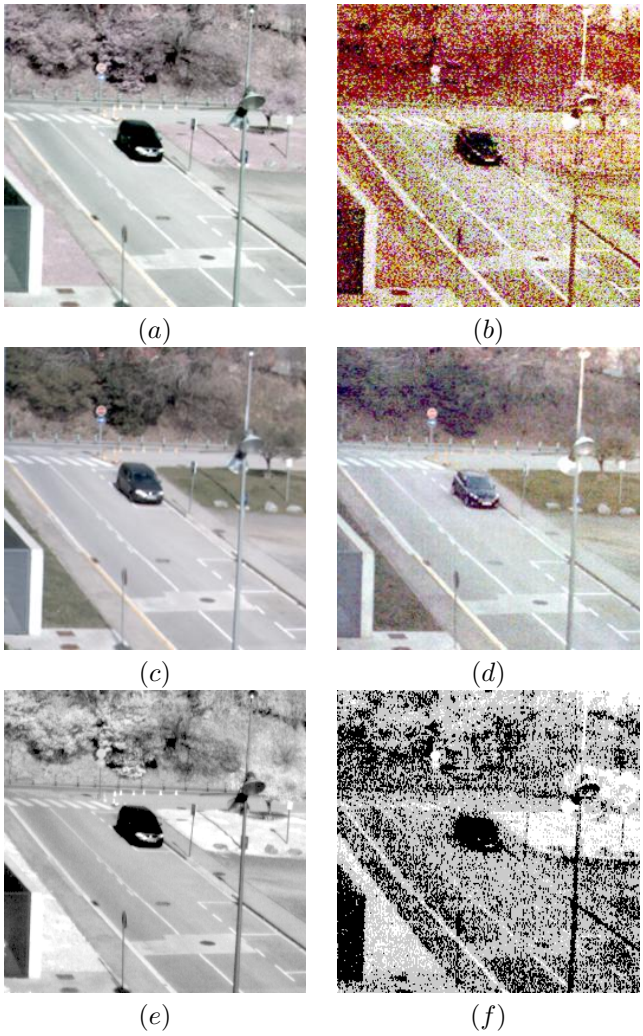

Fig. 3. Pair of images captured with hight/low lightness (see Fig. 2 (a)). (top) RGB with NIR information, note how vegetation regions (a) are more affected than the rest of objects present in the scene; (b) corresponds to a RGB (with NIR information) with a large mean Angular Error (AE) value. $(middle)$ Ground truth images (RGB images obtained with the usage of an Infrared Cut Off Filter); $(bottom)$ the corresponding NIR images.

to learn a mapping function $\Omega : \mathbb{R}^4 \rightarrow \mathbb{R}^3$. The proposed network, in addition to the input and output layers, consists of two hidden layers with 256 neurons each. In the training stage the weight hyper-parameters were centered in -0.08 (mean) and 0.25 (standard deviation).

The proposed neural network is trained using Adam Optimizer; the learning rate was set to 3×10^{-4} and weight decay to 1×10^{-5}, number of iterations were set to 1000. The two hidden layers used ReLU; the output of the network consists of a fully-connected layer. We opted for this kind of network structure because it is fast at train-test time and it can be replied with cheap GPUs or CPUs. After color restoration, some image enhancement algorithms were used to make a more suitable image for display to human vision; the processes were: linear stretching, simple white balance, simple gamma correction and finally bicubic demosaicing.

IV. Experimental Results

This section explains the evaluation procedure followed in order to assess the proposed color restoration neural network in the collected SSOMSI dataset. It must be noted that in most of the approaches presented in Section II color correction is performed by using a precomputed function (for instance the color correction matrix), which is not capable of automatically adapting itself to the amount on NIR information present in a given scene. For the NN training and testing process, as mentioned above, the whole set of 150 MS images from SSOMSI were considered; 135 images for training and 15 for testing. The image size are: 256×256×3 in RGB (ground truth) and 256×256×4 in RGBN.

The above mentioned multidimensional matrices were resized such as: $[R, G, B, N] = [R_{256\times256}, G_{256\times256}, B_{256\times256}, N_{256\times256}]$ for the input layer; similarly with the GT matrices. The NN model was implemented by TensorFlow computation library on a 16 GB RAM computer with 8 Cores i7 CPU. The GPU consisted of a NVIDIA Titan X. The training-testing process took about eight hours.

Due to the fact that there are no standard criteria to evaluate such a kind of single scene dataset, we used two evaluation metrics: $i)$ Angular Error (AE); and $ii)$ CIE color difference

2000 (ΔE_{00}), which are commonly used in color related literature. For each metric, we compared their values before and after the process of image restoration. These results can be observed quantitatively in Table I and qualitatively in Fig. 4.

TABLE I
ANGULAR ERRORS (AE) AND $\Delta Epr_{[0,10]}$ FOR THE SET OF SSOMSI. THE COMPARISON IS WITH NIR INFECTED RGB IMAGES (*column "Before"*) AND RGB IMAGES AFTER COLOR CORRECTION (*column "After"*).

Image #	AE		$\Delta Epr_{[0,10]}\%$	
	Before	After	Before	After
1	2.50	2.41	76.37	93.24
2	2.13	1.59	72.47	93.87
3	2.34	1.46	77.30	95.08
4	1.90	1.26	75.32	95.10
5	1.81	1.35	72.25	96.04
6	1.87	1.34	70.06	95.04
7	1.90	1.37	67.57	95.82
8	1.83	1.71	68.25	71.19
9	1.83	1.36	71.83	93.82
10	2.57	2.11	59.68	81.51
11	2.029	1.59	58.72	82.72
12	2.10	1.62	64.60	77.09
13	2.88	2.63	37.17	68.96
14	2.41	2.56	45.95	44.34
15	2.47	3.18	32.17	23.42

Table I presents quantitative evaluations, measured at every pixel; the angular error is computed between the obtained result (restored RGB image: RGB_{Rest}) and the corresponding RGB ground truth image (RGB_{GT}); the CIE color difference (ΔE_{00}) is also computed between the ground truth and the color corrected image. The angular error value is obtained as follow:

$$AE = \cos^{-1}\left(\frac{\text{dot}(RGB_{Rest}, RGB_{GT})}{\text{norm}(RGB_{Rest}) * \text{norm}(RGB_{GT})}\right) \quad (4)$$

This angular error (AE) is computed over every single pixel of the whole set of image patches (15 pairs) and used for comparisons with $RGB_{VIS+NIR}$ image (a RGB with NIR additional information). In addition to the angular error, the color difference ΔE_{00} is computed based on the CIELAB color space representation of the given image pairs; for every pair of pixels (LAB_{Rest_i}, LAB_{GT_i}), the color difference ΔE_{00_i} is computed as follow:

$$\Delta E_{00_i} = \left[\left(\frac{\Delta L'}{k_L S_L}\right)^2 + \left(\frac{\Delta C'}{k_C S_C}\right)^2 + \left(\frac{\Delta H'}{k_H S_H}\right)^2 + R_T\left(\frac{\Delta C'}{k_C S_C}\right)\left(\frac{\Delta H'}{k_H S_H}\right)\right]^{\frac{1}{2}} \quad (5)$$

where $\Delta L'$, $\Delta C'$ and $\Delta H'$ are the CIELAB lightness, chroma and hue differences, respectively. S_L, S_C, and S_H are weighting functions for the lightness, chroma and hue components. The k_L, k_C and k_H values are the parametric factors to be adjusted according to different viewing parameters. Finally, the R_T function is intended to improve color difference equation

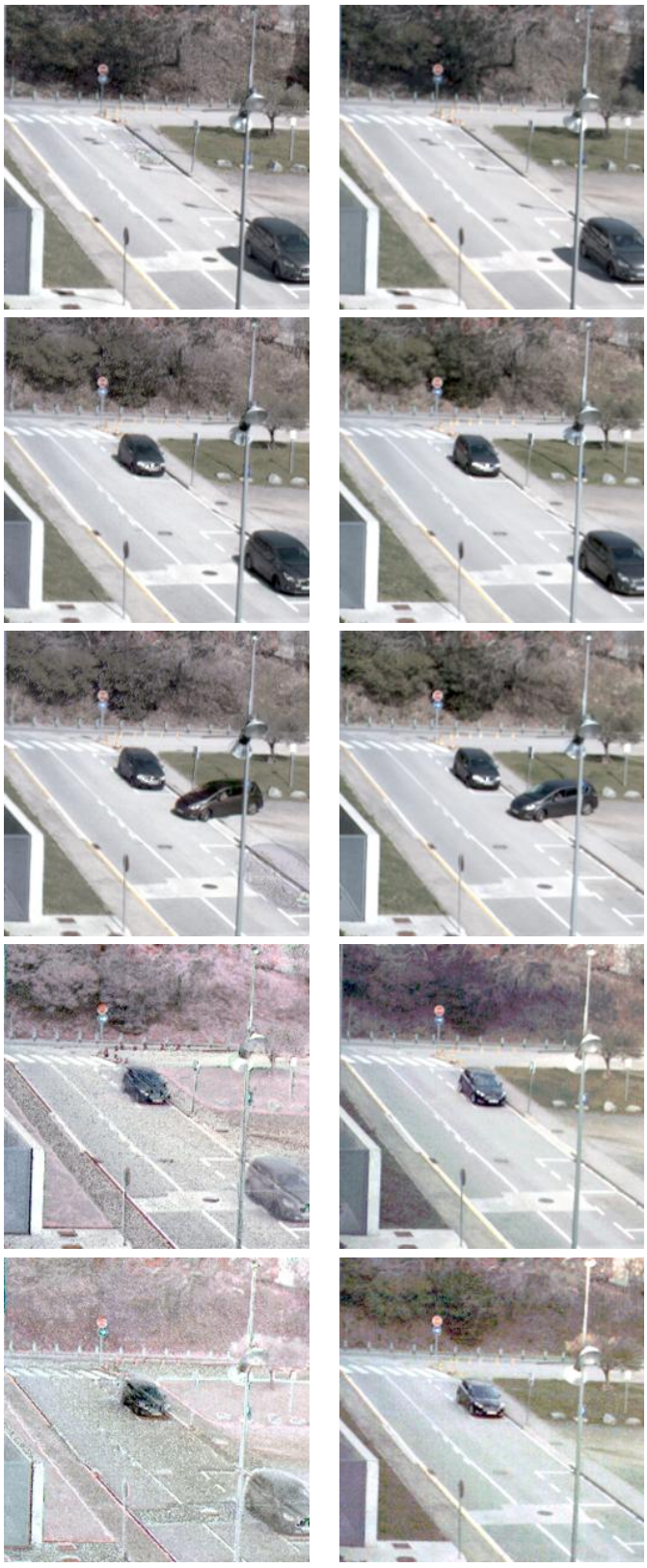

Fig. 4. Five different examples to qualitatively evaluate results from the proposed color correction approach (image number: 3, 7, 8, 14 and 15, from top to bottom, in Table I). Left column corresponds to the obtained results while right column corresponds to ground truth images.

for fitting chromatic differences in the blue region, for a more detailed description of Eq. 5 see [22] and [23]. Once computed ΔE_{00_i} values for the whole set of pixels (WP= image width $\times$ image height) of the given pair of images, the values presented in Table I are obtained as follow:

$$sp = 0$$
$$sp = \sum_{i=1}^{WP} \begin{cases} sp+1 & \text{if } a \leq \Delta E_{00_i} \leq b \\ sp & \text{otherwise} \end{cases}$$
$$\Delta Epr_{[a,b]} = \frac{sp \times 100}{WP} \quad (6)$$

where $\Delta Epr_{[a,b]}$ is the percentage of whole CIE color difference ΔE_{00_i} values in a range from a to b; more specifically, in the current work the range between [0,10] has been considered.

The restored RGB_{Rest} images and their corresponding ground truths were converted to the CIELAB color space before computing Eq. 5. The obtained WP ΔE_{00_i} values are measured in Eq. 6. According to the literature, a ΔE_{00_i} value in a range of 0 till 1 indicates that the difference of the two tested pixels are not perceptible for the human eyes and ΔE_{00_i} in a range 1 till 2 is perceptible through close observation; finally, the range [2, 10] is perceptible at a glance. Therefore, we have selected values in a range of 0 to 10. As mentioned above, this $\Delta Epr_{[a,b]}$ values correspond to those pixels with in the range [0,10]

From the results in Table I it can be appreciated that images without color restoration, in their majority, get the worst results independently of the evaluation metrics. Just the last two images (captured between 17:30 to 18:30) get better results with angular error and ΔE_{00}. Analyzing more deeper, when ΔE_{00} is used as an evaluation metric, more than 50% images tested have more that 90% of its pixels in the range of [0, 10]. It means that such image colors are close similar to the ground truth. In order to visually appreciate these results Fig. 4 presents just five results from the 15 pairs used for validation (the whole of corrected images can be found in the link of the data set presented above).

V. Conclusion

The RGB color restoration of a single sensor MS image is a challenging task with many of its troublesome issues being revealed in images of outdoor scenes. The amount of the NIR information affecting the RGB channels depends on several factors (e.g., daytime, composition of objects in the scene, exposition time, etc.). Hence, due to these complexities it is probable that a solution based on Neural Network must be sought in order to successfully address the nonlinearities involved in the problem of color restoration. In general, images that are captured under sufficient amount of sunlight are better restored in comparison to those with a lower amount of illumination. This could be due to the lack of images with low light during the training stage. As a future work larger data sets will be generated to better evaluate this problem.

References

[1] Z. Chen, X. Wang, and R. Liang, "Rgb-nir multispectral camera," *Optics express*, vol. 22, no. 5, pp. 4985–4994, 2014.

[2] L. Schaul, C. Fredembach, and S. Süsstrunk, "Color image dehazing using the near-infrared," in *Image Processing (ICIP), 2009 16th IEEE International Conference on*. IEEE, 2009, pp. 1629–1632.

[3] H. Yamashita, D. Sugimura, and T. Hamamoto, "Enhancing low-light color images using an rgb-nir single sensor," in *2015 Visual Communications and Image Processing (VCIP)*, Dec 2015, pp. 1–4.

[4] V. Tsagaris and V. Anastassopoulos, "Multispectral image fusion for improved rgb representation based on perceptual attributes," *International Journal of Remote Sensing*, vol. 26, no. 15, pp. 3241–3254, 2005.

[5] A. R. Petach, M. Toomey, D. M. Aubrecht, and A. D. Richardson, "Monitoring vegetation phenology using an infrared-enabled security camera," *Agricultural and Forest Meteorology*, vol. 195, pp. 143–151, 2014.

[6] N. J. Cuper, J. H. Klaessens, J. E. Jaspers, R. de Roode, H. J. Noordmans, J. C. de Graaff, and R. M. Verdaasdonk, "The use of near-infrared light for safe and effective visualization of subsurface blood vessels to facilitate blood withdrawal in children," *Medical engineering & physics*, vol. 35, no. 4, pp. 433–440, 2013.

[7] D. Yi, R. Liu, R. Chu, Z. Lei, and S. Z. Li, "Face matching between near infrared and visible light images," in *International Conference on Biometrics*. Springer, 2007, pp. 523–530.

[8] M. Martinello, A. Wajs, S. Quan, H. Lee, C. Lim, T. Woo, W. Lee, S. S. Kim, and D. Lee, "Dual aperture photography: Image and depth from a mobile camera," in *2015 IEEE International Conference on Computational Photography (ICCP)*, April 2015, pp. 1–10.

[9] A. Guidi, R. Achanta, C. Fredembach, and S. SÃ¼sstrunk, "Gui-aided nir and color image blending," in *Melecon 2010 - 2010 15th IEEE Mediterranean Electrotechnical Conference*, April 2010, pp. 1111–1116.

[10] K. Barnard, V. Cardei, and B. Funt, "A comparison of computational color constancy algorithms. i: Methodology and experiments with synthesized data," *IEEE transactions on Image Processing*, pp. 972–984, 2002.

[11] Q. Yan, X. Shen, L. Xu, S. Zhuo, X. Zhang, L. Shen, and J. Jia, "Cross-field joint image restoration via scale map," in *Proceedings of the IEEE International Conference on Computer Vision*, 2013, pp. 1537–1544.

[12] X. Shen, Q. Yan, L. Xu, L. Ma, and J. Jia, "Multispectral joint image restoration via optimizing a scale map," *IEEE transactions on pattern analysis and machine intelligence*, vol. 37, no. 12, pp. 2518–2530, 2015.

[13] D. Kiku, Y. Monno, M. Tanaka, and M. Okutomi, "Simultaneous capturing of rgb and additional band images using hybrid color filter array." in *Digital Photography*, 2014, p. 90230V.

[14] H. Teranaka, Y. Monno, M. Tanaka, and M. Ok, "Single-sensor rgb and nir image acquisition: Toward optimal performance by taking account of cfa pattern, demosaicking, and color correction," *Electronic Imaging*, vol. 2016, no. 18, pp. 1–6, 2016.

[15] C. Park and M. G. Kang, "Color restoration of rgbn multispectral filter array sensor images based on spectral decomposition," *Sensors*, vol. 16, no. 5, p. 719, 2016.

[16] C. H. Park, H. M. Oh, and M. G. Kang, "Color restoration for infrared cutoff filter removed rgbn multispectral filter array image sensor." in *VISAPP (1)*, 2015, pp. 30–37.

[17] M. Brown and S. Süsstrunk, "Multi-spectral sift for scene category recognition," in *Computer Vision and Pattern Recognition (CVPR), 2011 IEEE Conference on*. IEEE, 2011, pp. 177–184.

[18] J. Lüthen, J. Wörmann, M. Kleinsteuber, and J. Steurer, "A rgb/nir data set for evaluating dehazing algorithms," *Electronic Imaging*, vol. 2017, no. 12, pp. 79–87, 2017.

[19] C. Aguilera, X. Soria, A. Sappa, and R. Toledo, "Rgbn multispectral images: a novel color restoration approach," in *2017 15th International Conference on Practical Applications of Agents and Multi-Agent Systems(PAAMS)*. Springer, Advances in Ingelligent Systems and Computing, July 2017.

[20] G. Evangelidis, "Iat: A matlab toolbox for image alignment," 2013.

[21] H. A. Khan, J.-B. Thomas, J. Y. Hardeberg, and O. Laligant, "Illuminant estimation in multispectral imaging," *JOSA A*, vol. 34, no. 7, pp. 1085–1098, 2017.

[22] G. Sharma, W. Wu, and E. N. Dalal, "The CIEDE2000 color-difference formula: Implementation notes, supplementary test data, and mathematical observations," *Color Research & Application*, vol. 30, no. 1, pp. 21–30, 2005.

[23] M. R. Luo, G. Cui, and B. Rigg, "The development of the cie 2000 colour-difference formula: Ciede2000," *Color Research & Application*, vol. 26, no. 5, pp. 340–350, 2001.